The Role of Excited Electronic States in Hypervelocity Collisions: Enhancement of the O(3P) + HCl → OCl + H Reaction Channel

ARTICLE *in* JOURNAL OF PHYSICAL CHEMISTRY LETTERS · SEPTEMBER 2010

Impact Factor: 7.46 · DOI: 10.1021/jz1011059

THE JOURNAL OF PHYSICAL CHEMISTRY Letters

pubs.acs.org/JPCL

The Role of Excited Electronic States in Hypervelocity Collisions: Enhancement of the O(^{3}P) + HCl → OCl + H Reaction Channel

Andrew J. Binder,[†] Richard Dawes,*[,‡] Ahren W. Jasper,[§] and Jon P. Camden*[,†]

[†]Department of Chemistry, University of Tennessee, Knoxville, Tennessee 37996-1600, [‡]Missouri University of Science and Technology, Rolla, Missouri 65409, and [§]Combustion Research Facility, Sandia National Laboratories, P.O. Box 969, Livermore, California 94551

ABSTRACT The role of excited electronic states in the O + HCl reaction was studied using the quasi-classical trajectory method for collision energies between 1 and 5.5 eV. Global potential energy surfaces were developed for the ground (^{3}A″) and first excited (^{3}A′) electronic states of the OHCl system using an interpolating moving least-squares-based method for energies up to 6.5 eV above the reactant valley. High-accuracy ab initio data were computed at automatically selected points using an 18-electronic-state model and the generalized dynamically weighted multireference configuration interaction (GDW-MRCI) method extrapolated to the complete basis set limit. The results show significant dynamical differences between ground- and excited-state reactions. At high collision energies, over half of the total OCl reactive flux originates from reactions on the ^{3}A′ state, whereas OH is produced almost exclusively by the ^{3}A″ state. Inclusion of the excited electronic state, therefore, dramatically alters the OCl/OH product branching ratio.

SECTION Dynamics, Clusters, Excited States

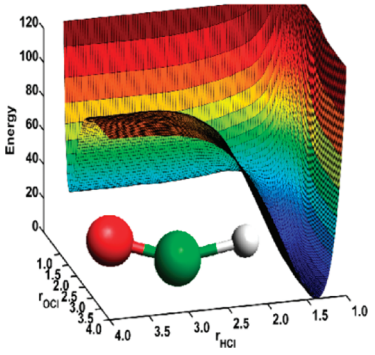

Hyperthermal collisions are known to occur frequently in extreme environments, such as those found in rocket plumes and around space vehicles in low earth orbit.[1] These high-energy collisions give rise to effects not usually observed in thermal systems, such as the dominance of highly endothermic reaction pathways and unexpected mechanisms.[2−6] A recent study, for example, by Gimelshein et al.[7] shows that the O + HCl reaction plays an important role in reactive flows that result from the interaction of jet aircraft with the atmosphere at high altitudes. At hyperthermal energies, the O + HCl reaction may follow three main pathways

$$O(^3P) + HCl \rightarrow OH + Cl \quad \Delta H^\circ_{f,0} = 0.021 \text{ eV} \quad (1)$$

$$\rightarrow OCl + H \quad \Delta H^\circ_{f,0} = 1.687 \text{ eV} \quad (2)$$

$$\rightarrow O + H + Cl \quad \Delta H^\circ_{f,0} = 4.431 \text{ eV} \quad (3)$$

Zhang et al.[5,6] have shown experimentally that the threshold for reaction 2 is ∼2 eV, and calculations suggest that it quickly becomes the dominant pathway as collision energy increases.[5] This feature of the O + HCl reaction highlights the fact that highly endothermic reaction channels can be more efficient than lower-energy pathways at hyperthermal collision energies. Despite this fact, the dynamics of high-energy collisions, especially the role of electronic excited states, remains mostly unexplored.

Potential energy surfaces (PESs) describing reaction 1 on the ground (^{3}A″) and first excited triplet states (^{3}A′) of the OHCl system were constructed by Ramachandran and Peterson.[8] Xie et al. subsequently performed thermal reactive scattering calculations on these surfaces and found that the excited state does not contribute significantly to the OH + Cl product channel cross section.[9] This result was attributed to the small cone of acceptance for the H-abstraction channel on ^{3}A′. Although previous theoretical studies of the O + HCl → OCl + H channel were restricted to the ground triplet state, Camden and Schatz[4] showed that the cone of acceptance is also smaller for the reaction of O with HCl on the first excited triplet state, which suggested a similarly small contribution to the OCl product from reactions on the excited state.

In this work, we calculate high-accuracy global ^{3}A″ and ^{3}A′ PESs of the OHCl system in a 6.5 eV energy range capable of describing all possible reactive channels on the lowest-energy triplet states. We then perform dynamics calculations on these surfaces to assess the relative importance of the ^{3}A″ and ^{3}A′ electronic states in determining cross sections for all three reaction paths. Quasi-classical trajectory calculations show, surprisingly, that reactions forming OCl proceed with equal efficiently on both the A′ and A″ surfaces, whereas reactions forming OH are suppressed on the excited-state surface. This feature of the dynamics leads to a dramatic increase in the ratio of OCl to OH products with increasing energy.

Received Date: August 6, 2010
Accepted Date: September 14, 2010

DOI: 10.1021/jz1011059 | *J. Phys. Chem. Lett.* **2010**, *1*, 2940–2945

The lowest-lying states for the $O(^3P) + HCl(^1\Sigma^+)$ supersystem are three triplet molecular electronic states that are asymptotically degenerate (neglecting spin−orbit interactions). Approach of the oxygen atom (considering C_s symmetry for generality) separates the three triplet 1A″, 1A′, and 2A″ states, although there is a Renner−Teller pairing of the A′ and A″ states with associated degeneracy at linear configurations. While the PESs developed for this study do not include spin−orbit coupling interactions, the adiabatic correlations of the fine-structure states were determined in order to apply the correct statistical weighting to the computed cross sections. The spin−orbit interaction of the $O(^3P)$ atom produces nine fine-structure states in three levels ($^3P_2$, $^3P_1$, and $^3P_0$) that have degeneracies of 5, 3, and 1 respectively. Electronic structure calculations including fine structure show that the $O(^3P)$ spin−orbit splittings become negligible in the molecular region and that these components correlate to the molecular OHCl states as follows: three components of the $^3P_2$ state correlate to 1A″, two components of $^3P_2$ and one component of $^3P_1$ correlate to 1A′, and two components of $^3P_1$ along with the lone $^3P_0$ state correlate to 2A″.

To determine the total reaction cross sections, we first calculated the cross sections using adiabatic (Born−Oppenheimer) molecular dynamics on the A″ and A′ surfaces. Individual electronic-state cross sections were then weighted using a Boltzmann distribution assuming the high-temperature limit for the $O(^3P)$ spin−orbit states, resulting in a one-third weighting for each molecular state, consistent with the correlation between the $O(^3P)$ states and the OHCl molecular states described above. Application of the low-temperature limit in this model would place three-fifths and two-fifths weight on the ground and excited states, respectively. The 2A″ state was excluded from consideration in this study since it does not correlate adiabatically to the ground-state OCl product. Quantification of nonadiabatic interactions involving 2A″ or states of other spin multiplicities is an avenue for future research.

Cross sections for the OCl + H and OH + Cl reaction pathways as well as the ratio OCl/OH are shown in Figure 1. In good agreement with previous studies,[9] we find that $^3A'$ makes only a small contribution to the total OH + Cl reaction cross section. In sharp contrast to this result for the OH channel, we find that production of OCl is quite efficient in the excited state. Inclusion of the first excited state nearly doubles the ratio of OCl to OH products at 5.5 eV when compared to calculations that include only the ground-state reactivity. These results highlight the potential for electronic excited states to selectively enhance one particular reaction channel and suggest that calculation of accurate branching ratios between H-atom abstraction and elimination requires inclusion of excited-state dynamics.

The ratio of OH to OCl products has been measured by Minton and co-workers.[6] At a collision energy of 3 eV, their experiment yields an OH/OCl ratio of 1.5, which is within the range of our calculations which include the high T (OH/OCl = 1.4) and low T (OH/OCl = 1.5) limits. Agreement is much improved over the previous B3LYP result of 2.4 for this collision energy. At 4 eV, the experimental ratio (OH/OCl) was measured at 0.8, compared to values of 0.49 and 0.43

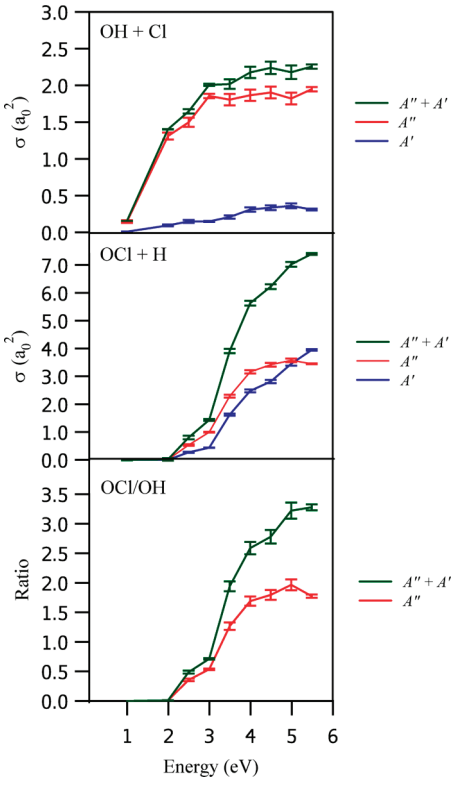

Figure 1. Theoretical cross sections (green) for O + HCl (v = 0, J = 0) → OH + Cl (top) and O + HCl → OCl + H (middle) reaction channels showing the contributions from the ground triplet (red) and first excited triplet (blue) states. Cross sections were calculated assuming adiabatic reaction dynamics on the 1A′ and 1A″ states with weightings calculated from a Boltzmann distribution of the O atom states at the high T limit and assuming that the 2A″ state does not lead to reactive trajectories. Bottom: Ratio of OCl product channel to the OH product channel (σ_{OCl}/σ_{OH}). Note that the addition of the A′ state has a significant impact on the ratio of OCl/OH.

from the present calculations in the low and high T limits, respectively, and 1.2 for the previous B3LYP calculation. The calculated ratio is quite sensitive to the energetics of the competing channels on the various PESs. The B3LYP method underestimates the barrier to OH formation by ∼9 kcal/mol (almost barrierless) and thus may overestimate the OH cross section and hence overestimate the OH:OCl ratio. The MRCI surface, while greatly improved, overshoots the best estimate of the reaction barrier to OH by ∼1.05 kcal/mol,[8] which may result in an underestimation of the OH cross section and hence a smaller OH/OCl ratio than observed. The most significant neglected contributions to the energetics in the present PES are core−valence correlation and spin−orbit corrections. Quantitative prediction of the OH/OCl ratio at all energies may require further refinement of the PES and possibly a more sophisticated treatment of the dynamics. The ratio of OH/OCl is also influenced by the initial O-atom fine structure state distribution, which provides the relative weightings of A′ and A″ in these calculations. Experimental measurements taken with a range of initial O-atom temperatures could shed more light on the roles of excited states and nonadiabatic dynamics.

DOI: 10.1021/jz1011059 | J. Phys. Chem. Lett. 2010, 1, 2940–2945

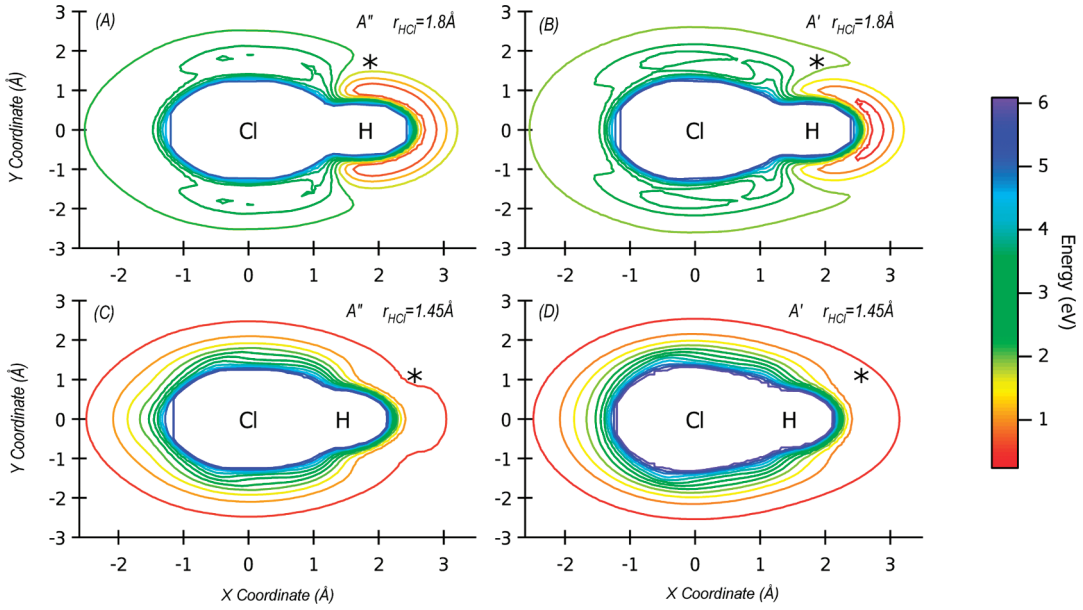

Figure 2. Potential energy surface contour plots for the O + HCl reaction with the H−Cl bond lengths fixed at r_{HCl} = 1.8 (top) and 1.45 Å (bottom) on the ground triplet (left) and first excited triplet (right) states. The zero of potential energy corresponds to the bottom of the reactant valley with the O atom placed at infinity. The difference in shapes between A″ and A′ correspond to the bent transition states on A″ as well as the linear transition states on A′.

In order to explore the origin of channel specific reactivity on the different surfaces, we plot in Figure 2 the PESs for fixed H−Cl bond length, which is set at the average of the H−Cl bond lengths on the A″ and A′ transition-state H−Cl lengths for the OCl (r_{HCl} = 1.8 Å) and OH (r_{HCl} = 1.45 Å) channels. The transition-state HCl bond lengths are very similar between the two surfaces for a given channel (Table 1). The "dents" seen in Figure 2a and c (denoted by the stars) correlate to the bent shape of the O−H−Cl and O−Cl−H transition states on A″. However, reactions at high energy need not follow the minimum-energy path, and the influence of the transition state may be less important.[10,11] The excited-state surface is generally higher in energy than the ground-state surface at all coordinates, but more importantly, it exhibits a smaller cone of acceptance for the approaching O atom. The reaction channel leading to OH products is known to be dominated by a stripping mechanism[6] which occurs at higher impact parameter, meaning that much of the collision energy is placed into orbital angular momentum. Therefore, the smaller cone of acceptance around the H atom and the linear transition state on the excited state acts to suppress the stripping mechanism on the excited state, leading to a lower cross section for that reaction channel.

Two major dynamical differences may be responsible for the lack of a similarly lower cross section for the OCl channel on A′. Unlike the OH reaction channel, the OCl channel is dominated by low impact parameter "head on" collisions.[5,6] While the potential surface does increase in energy around the Cl atom, there is more than enough energy in direct collision to overcome the higher reaction barrier, and thus, the OCl pathway is efficient on both surfaces. The relative size of the Cl atom to the H atom also presents the oncoming O atom a much larger target for collision. These two differences work to offset the smaller cone of acceptance for the A′ OCl channel.[4]

Table 1. Relative Energies of Asymptotes, Transition Structures, and van der Waals Complexes for the Two Reaction Paths[a]

Reaction Path 1: O + HCl → OH + Cl

structure	ΔV	r_{HCl}	r_{OH}	θ_{OHCl}
O + HCl	0.00	1.275	8.000	
O−HCl (vdw)	−1.73	1.278	2.247	180.00
O−H−Cl (TS 1)	11.65	1.443	1.242	132.57
O−H−Cl (TS 1)[b]	14.96	1.463	1.195	180.00
OH−Cl (vdw)	−6.04	2.365	0.973	69.24
OH + Cl	1.07	8.000	0.969	

Reaction Path 2: O + ClH → OCl + H

structure	ΔV	r_{HCl}	r_{OCl}	Θ_{OClH}
O + ClH	0.00	1.275	8.000	
O-ClH (vdw)	−0.89	1.277	3.350	150.29
O−Cl−H (TS 2)	47.45	1.935	1.600	156.95
O−Cl−H (TS 2)[b]	49.06	1.773	1.643	180.00
OCl−H (vdw)	43.84	2.818	1.579	180.00
OCl + H	44.13	8.000	1.577	

[a] Energies are in kcal/mol, and distances are in Angstroms. All energies relative to O + HCl asymptote. Tabulated values are not zero-point-corrected. [b] Transition structures on A′ excited electronic state.

Significant differences in reaction dynamics are also seen between the A′ and A″ surfaces. Figure 3 shows plots of the differential cross section (DCS) for each reaction pathway on the ground and excited PESs at 3 and 5.5 eV. Product OH scattering into the extreme forward direction ($\cos(\theta) > 0.8$) is reduced significantly on the A′ state and supports the idea that

DOI: 10.1021/jz1011059 | J. Phys. Chem. Lett. 2010, 1, 2940–2945

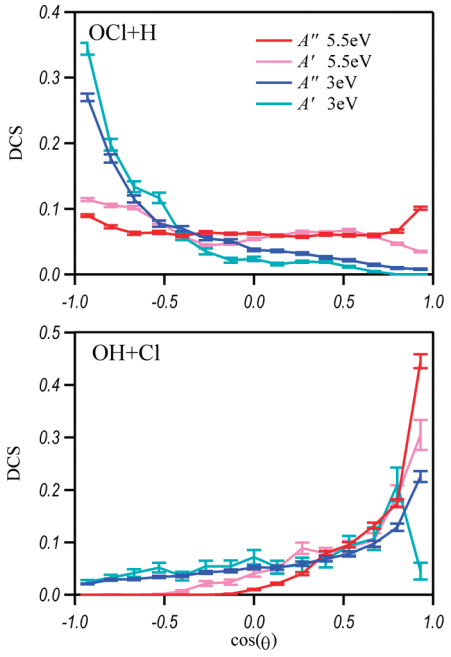

Figure 3. Differential cross sections for the OCl (top) and OH (bottom) product channels on the A′ and A″ states at 3 and 5.5 eV. Distributions are normalized such that the area under the curve is equal to 1.

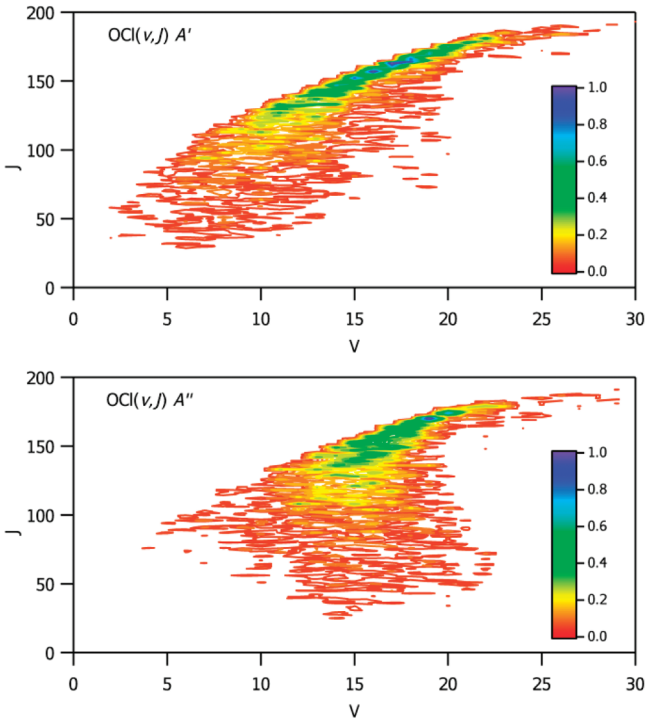

Figure 4. Contour plots showing the rovibrational state distribution of the OCl product diatom at E_{coll} = 5.5 eV for A′ (top) and A″ (bottom). Data are plotted as a probability distribution, where the highest probability is set to 1. Note that at low rotational states, the A′ surface causes a shift toward lower vibrational states.

the reduced OH reactivity on A′ originates from the smaller cone of acceptance and nature of the transition state. Dynamical differences can also be seen in the rovibrational (v,J) state distribution of the OCl products (Figure 4). Reactions on A′ show a distinct shift toward lower v-states at low J-states for the OCl pathway when compared to the distribution on the A″ state, suggesting that this region would be ideal for experiments attempting to probe reactions originating solely from the ^{3}A′ electronic excited state.

This study illustrates the importance of including the A′ state in the calculation of cross sections, product branching ratios, and dynamical quantities for the O + HCl reaction at hyperthermal energies. Our trajectory calculations suggest that the two main hyperthermal reaction pathways, that is, those leading to OCl + H or OH + Cl products, proceed quite differently on the first excited electronic state. Differences in the two potential energy surfaces suggests a suppression of the dominant stripping mechanism for the OH + Cl reaction channel on the excited state. Without a similar suppression mechanism on A′ for the OCl channel, the ratio of OCl to OH reaction products increases significantly. Unlike the OH + Cl channel, the first excited-state contribution is comparable to that of the ground state and cannot be reasonably neglected in calculation of the overall reaction cross section. We expect this effect to be general to hyperthermal reactions of O(^{3}P) that lead to H-atom elimination.

COMPUTATIONAL METHODS

An interpolating moving least-squares (IMLS)-based PES generator was used to separately construct ^{3}A″ and ^{3}A′ surfaces from automatically calculated ab initio data,[12] with internuclear distances chosen as the coordinates. The fit was restricted to internuclear distances of less than 8 Å and energies up to 6.5 eV above the O(^{3}P) + HCl reaction valley. The PESs describe all three reaction channels, including complete fragmentation. Given the large configuration space and energy range, a generous number (∼4000) of ab initio energy data points were included in each fit. The resulting PESs provide analytic gradients of the fit, which promotes excellent energy conservation in QCT studies.

The ab initio data used in the fits were computed using an 18-state model, reflecting the asymptotic degeneracy of triplet electronic states for the three separate atoms. The Molpro electronic structure code was used for all of the calculations.[13] First, the set of 18 triplet electronic states (8A′, 10A″) were included in a generalized dynamically weighted state-averaged CASSCF (GDW-SA-CASSCF) calculation.[14,15] The β parameter (used in the energy-dependent functional in the GDW scheme) was set to 3.0 eV. A separate calculation was performed for the ground ^{3}A″ and excited ^{3}A′ states, with maximum weight focused on the state of interest in each case and weights for other states determined by the GDW scheme.[15] Next, this was used as the reference for a Davidson-corrected multireference configuration interaction (MRCI+Q) calculation.[16,17] The CBS limit was estimated from two zeta levels using the l^{-3} formula[18] and the aug-cc-pV(T+d)Z and aug-cc-pV(Q+d)Z bases, where +d indicates additional tight d functions for the chlorine atom.[19] A full-valence active space was used, except that the 2s orbitals on oxygen and the 3s orbitals on chlorine were closed in the CASSCF calculations

DOI: 10.1021/jz1011059 | J. Phys. Chem. Lett. 2010, 1, 2940–2945

(this restriction was lifted for the MRCI calculations). Energies and geometries for relevant structures on the two PESs are reported in Table 1 and Supporting Information (Table S-1).

The application of IMLS fitting to trajectory calculations has been described in a previous publication;[20] therefore, we provide only specific details and changes to the method here. Several methods for semiclassical quantization have been described for the QCT method.[21,22] In the current study, the classical action variables, corresponding to the initial quantum state (v,J), for the diatom were found using the method of Porter, Raff, and Miller[21] with Morse alpha parameters, α, fitted using fixed well depths, D_e, and equilibrium bond lengths, r_e, from the potential surface. Quantitative agreement was found between analyses of trajectories calculated using the Porter, Raff, and Miller method and the previous method of random sampling of vibrational phases from a single diatomic trajectory of the HCl diatom. Trajectories were then run in batches of 10 000 or more with a maximum impact parameter, b_{max}, of 6 a_0, an initial O + HCl separation of 11 a_0, and an integration time step of 6 au. Batches were run using collision energies, E_{coll}, between 1 and 5.5 eV on both the ground, (^{3}A″) and first excited (^{3}A′) triplet states. Integration was terminated when the distance between any two atoms exceeded 13 a_0. Rovibrational quantum state analysis was performed on the product diatoms for reactions leading to OH and OCl. The rotational quantum number, J, was obtained by calculating the angular momentum of the diatom in its center of mass frame, L_{CM}, in units of $\hbar$ and converting to the quantum number, J, using the standard quantum mechanical expression $L^2 = J(J+1)$. The vibrational quantum number, v, was then calculated using the prescription provided by Porter, Raff, and Miller (eq 49 of ref 3 with a correction provided by Geiger and Schatz[23]) and the appropriate Morse parameters. Binning was done by rounding the resulting J or v to the nearest integer.

SUPPORTING INFORMATION AVAILABLE

A table listing calculated disassociation energies and bond lengths as well as additional plots of the ^{3}A′ and ^{3}A″ PESs at fixed bond angles. This material is available free of charge via the Internet at http://pubs.acs.org.

AUTHOR INFORMATION

Corresponding Author:

*To whom correspondence should be addressed. E-mail: dawesr@mst.edu (R.D.); jcamden@utk.edu (J.P.C.).

ACKNOWLEDGMENT R.D. and A.W.J. are supported by the Division of Chemical Sciences, Geosciences, and Biosciences, the Office of Basic Energy Sciences, the U.S. Department of Energy; Sandia is a multiprogram laboratory operated by Sandia Corporation, a Lockheed Martin Company, for the National Nuclear Security Administration under Contract DE-AC04-94-AL85000. R.D. thanks K. A. Peterson (Washington State) for useful discussions regarding the electronic structure of this system. This work is also supported by the University of Tennessee Knoxville (A.J.B. and J.P.C.). A.J.B. and J.P.C. thank George Schatz for useful discussions on the conversion of diatom quantum numbers to classical action variables.

REFERENCES

(1) Murad, E. Spacecraft Interaction with Atmospheric Species in Low Earth Orbit. *J. Spacecr. Rockets* **1996,** *33*, 131.

(2) Garton, D. J.; Minton, T. K.; Troya, D.; Pascual, R.; Schatz, G. C. Hyperthermal Reactions of O(^{3}P) with Alkanes: Observations of Novel Reaction Pathways in Crossed-Beams and Theoretical Studies. *J. Phys. Chem. A* **2003,** *107*, 4583–4587.

(3) Troya, D.; Schatz, G. C.; Garton, D. J.; Brunsvold, A. L.; Minton, T. K. Crossed Beams and Theoretical Studies of the O(^{3}P) + $CH_4 \rightarrow$ H + OCH_3 Reaction Excitation Function. *J. Chem. Phys.* **2004,** *120*, 731–739.

(4) Camden, J. P.; Schatz, G. C. Direct Dynamics Simulations of O(^{3}P) + HCl at Hyperthermal Collision Energies. *J. Phys. Chem. A* **2006,** *110*, 13681–13685.

(5) Zhang, J. M.; Camden, J. P.; Brunsvold, A. L.; Upadhyaya, H. P.; Minton, T. K.; Schatz, G. C. Unusual Mechanisms Can Dominate Reactions at Hyperthermal Energies: An Example from O(^{3}P) + HCl → ClO + H. *J. Am. Chem. Soc.* **2008,** *130*, 8896.

(6) Zhang, J. M.; Brunsvold, A. L.; Upadhyaya, H. P.; Minton, T. K.; Camden, J. P.; Garashchuk, S.; Schatz, G. C. Crossed-Beams and Theoretical Studies of Hyperthermal Reactions of O(^{3}P) with HCl. *J. Phys. Chem. A* **2010,** *114*, 4905–4916.

(7) Gimelshein, S. F.; Levin, D. A.; Alexeenko, A. A. Modeling of Chemically Reacting Flows from a Side Jet at High Altitudes. *J. Spacecr. Rockets* **2004,** *41*, 582–591.

(8) Ramachandran, B.; Peterson, K. A. Potential Energy Surfaces for the ^{3}A″ and ^{3}A′ Electronic States of the O(^{3}P) + HCl System. *J. Phys. Chem. A* **2003,** *119*, 9590–9600.

(9) Xie, T.; Bowman, J; Duff, J. W.; Braunstein, M.; Ramachandran, B. Quantum and Quasiclassical Studies of the O(^{3}*P*)+HCl -> OH+Cl(^{2}*P*) Reaction Using Benchmark Potential Surfaces. *J. Chem. Phys.* **2005,** *122*, 14301–14313.

(10) Yan, T. Y.; Doubleday, C; Hase, WL. A PM3-SRP Plus Analytic Function Potential Energy Surface Model for O(^{3}P) Reactions with Alkanes. Application to O(^{3}P) Plus Ethane. *J. Phys. Chem. A* **2004,** *108*, 9863–9875.

(11) Pomerantz, A. E.; Camden, J. P.; Chiou, A. S.; Ausfelder, F.; Chawla, N.; Hase, W. L.; Zare, R. N. Reaction Products with Internal Energy Beyond the Kinematic Limit Result from Trajectories Far from the Minimum Energy Path: An Example from H + HBr → H_2 + Br. *J. Am. Chem. Soc.* **2005,** *127*, 16368–16369.

(12) Dawes, R.; Wagner, A. F.; Thompson, D. L. *Ab Initio* Wavenumber Accurate Spectroscopy: CH_2 and HCN Vibrational Levels on Automatically Generated IMLS Potential Energy Surfaces. *J. Phys. Chem. A* **2009,** *113*, 4709–4721.

(13) Werner, H. J.; Knowles, P. J.; Lindh, R.; Manby, F. R.; Schütz, M.; et al. MOLPRO, version 2009.1; A Package of Ab Initio Programs; University College Cardiff Consultants Limited: Wales, U.K., 2009.

(14) Deskevich, M. P.; Nesbitt, D. J.; Werner, H. J. Dynamically Weighted Multiconfiguration Self-Consistent Field: Multistate Calculations for F + H_2O → HF + OH Reaction Paths. *J. Chem. Phys.* **2004,** *120*, 7281–7289.

(15) Dawes, R.; Jasper, A. W.; Tao, C; Richmond, C.; Mukarakate, C.; Kable, S. H.; Reid, S. A. Theoretical and Experimental Spectroscopy of the S_2 State of CHF and CDF: Dynamically Weighted Multireference Configuration Interaction Calculations for High-Lying Electronic States. *J. Phys. Chem. Lett.* **2010,** *1*, 641–646.

(16) Werner, H. J.; Knowles, P. J. An Efficient Internally Contracted Multiconfiguration Reference Configuration-Interaction Method. *J. Chem. Phys.* **1988,** *89*, 5803.

DOI: 10.1021/jz1011059 | *J. Phys. Chem. Lett.* **2010,** *1*, 2940–2945

(17) Knowles, P. J.; Werner, H. J. An Efficient Method for the Evaluation of Coupling-Coefficients in Configuration-Interaction Calculations. *Chem. Phys. Lett.* **1988,** *145*, 514.
(18) Helgaker, T.; Jorgensen, P.; Olsen, J. *Molecular Electronic Structure Theory*; Wiley: New York, 2000.
(19) Dunning, T. H.; Peterson, K. A.; Wilson, A. K. Gaussian Basis Sets for Use in Correlated Molecular Calculations. X. The Atoms Aluminum Through Argon Revisited. *J. Chem. Phys.* **2001,** *114*, 9244–9253.
(20) Camden, J. P.; Dawes, R.; Thompson, D. L. Application of Interpolating Moving Least Squares Fitting to Hypervelocity Collision Dynamics: $O(^3P) + HCl$. *J. Phys. Chem. A* **2009,** *113*, 4626–4630.
(21) Peslherbe, G. H.; Wang, H. B.; Hase, W. L. Monte Carlo Sampling for Classical Trajectory Simulations. *Adv. Chem. Phys.* **1999,** *105*, 171.
(22) Porter, R. N.; Raff, L. M.; Miller, W. H. Quasiclassical Selection of Initial Coordinates and Momenta for a Rotating Morse Oscillator. *J. Phys. Chem.* **1975,** *63*, 2214–2218.
(23) Geiger, L. C.; Schatz, G.C. A Quasiclassical Trajectory Study of Collisional Excitation in H + CO. *J. Phys. Chem.* **1984,** *88*, 214–221.

DOI: 10.1021/jz1011059 | *J. Phys. Chem. Lett.* **2010,** *1*, 2940–2945